

# FLAT FIELDS FOR THE CCD SPECTRAL MODES

---

Ralph Bohlin  
September 1999

---

## ABSTRACT

*Except for fringing effects at the longer wavelengths, the pixel-to-pixel flat field for the spectral modes is independent of wavelength but does change with time. An average flat with one to four million electrons/px is applicable to all CCD first order modes, except G750M, after the dust mote regions are inserted from separate low or medium dispersion flats. Application of this flat to spectra of standard stars produces a rms residual noise level as good as ~0.3%, which is comparable to the residual noise achievable with no flat. Since the intrinsic rms structure in the CCD flat field is 0.8%, those five current pipeline CCD flats that have less than 0.8% statistical significance produce spectra that are always noisier than with no flat. Since the time constant for changes in the CCD flat is some days, a contemporaneous flat with about a million electrons/px could enable observations with a S/N approaching 1000 for bright sources. For a stellar spectrum with Poisson S/N=1100, an actual S/N of 400 is demonstrated with the new flat.*

---

## 1. INTRODUCTION

Below  $\sim 6200\text{\AA}$  where there is no fringing, the STIS CCD has 0.8% rms intrinsic structure, which is independent of wavelength. In an extracted spectrum, the intrinsic structure is reduced to  $\sim 0.3\%$ . Thus, a high precision flat field correction becomes important for observational data with around 16,000 counts per pixel in the CCD image or around 100,000 counts per pixel in the extracted spectrum. For example in the ideal case of a non-variable flat field, a flat field with only 16,000 counts per pixel is the break-even point, where the signal-to-noise (S/N) of  $1/.008 = 125$  is the same with and without application of the flat. Because the current CCD pipeline flat fields are derived from laboratory data obtained in each of the different modes, there are disparities in the S/N and a variety of different artifacts among these first order low and medium dispersion pipeline flats. Five of these lab flats do not have sufficient counting statistics.

A desire for uniform high quality CCD spectral flats motivated this comprehensive study of the dependence of the flight flat fields on wavelength and time.

## 2. FLAT FIELD DATA PROCESSING

Table 1 lists the CCD flat field observations that have a high S/N. No G750 data is included in Table 1, because of fringing that extends as short as the G750M central wavelength setting of 6252Å. Dozens of G430M flat observations with the 52x2 slit are also ignored, because their total signal is comparable to the small set of 12 G430M, 50CCD observations from PROPID=7666, which do not have the complication of the fiducial bars on the 52x2 aperture. The G230LB and G230MB observations with the 52x2 aperture are excluded because of the much higher S/N in the G230 50CCD data.

**Table 1.** CCD OBSERVATIONS USED TO DEFINE THE FLAT FIELDS

ROOTNAME	MODE	APER	CENWAV	DETECTOR	LAMP	DATE	TIME	PROPID	EXPTIME	CR
O4LH04030	G230LB	50CCD	2375	CCDgain4	D2	05/03/98	06:13:13	7602	25.0	5
O3WL01010	G430L	52X2	4300	CCDgain1	TU	14/04/97	04:55:30	7142	150.0	3
O3WL01020	G430L	52X2	4300	CCDgain4	TU	14/04/97	05:02:06	7142	150.0	3
O3WL02010	G430L	52X2	4300	CCDgain1	TU	17/05/97	00:21:58	7142	60.0	3
O3WL02020	G430L	52X2	4300	CCDgain4	TU	17/05/97	00:27:04	7142	270.0	3
O3WL04010	G430L	52X2	4300	CCDgain1	TU	16/06/97	02:01:57	7142	60.0	3
O3WL04020	G430L	52X2	4300	CCDgain4	TU	16/06/97	02:07:03	7142	270.0	3
O44K01EKM	G430L	52X2	4300	CCDgain1	TU	14/07/97	13:12:15	7636	50.0	1
O44K01ELM	G430L	52X2	4300	CCDgain4	TU	14/07/97	13:14:27	7636	44.0	1
O44K02EPM	G430L	52X2	4300	CCDgain1	TU	12/08/97	06:54:04	7636	50.0	1
O44K02EXM	G430L	52X2	4300	CCDgain1	TU	12/08/97	06:56:16	7636	50.0	1
O44K02EYM	G430L	52X2	4300	CCDgain1	TU	12/08/97	06:58:28	7636	50.0	1
O44K02EZM	G430L	52X2	4300	CCDgain4	TU	12/08/97	07:00:40	7636	44.0	1
O44K02F0M	G430L	52X2	4300	CCDgain4	TU	12/08/97	07:02:46	7636	44.0	1
O44K02F1M	G430L	52X2	4300	CCDgain4	TU	12/08/97	07:04:52	7636	44.0	1
O44K03KKQ	G430L	52X2	4300	CCDgain1	TU	08/09/97	16:15:08	7636	50.0	1
O44K03KQQ	G430L	52X2	4300	CCDgain1	TU	08/09/97	16:17:20	7636	50.0	1
O44K03KRQ	G430L	52X2	4300	CCDgain1	TU	08/09/97	16:19:32	7636	50.0	1
O44K03KSQ	G430L	52X2	4300	CCDgain4	TU	08/09/97	16:21:44	7636	44.0	1
O44K03KTQ	G430L	52X2	4300	CCDgain4	TU	08/09/97	16:23:50	7636	44.0	1
O44K03KUQ	G430L	52X2	4300	CCDgain4	TU	08/09/97	16:25:56	7636	44.0	1
O44K04010	G430L	52X2	4300	CCDgain1	TU	12/10/97	04:08:00	7636	120.0	3
O44K04020	G430L	52X2	4300	CCDgain4	TU	12/10/97	04:14:06	7636	102.0	3

STIS Instrument Science Report 99-06

ROOTNAME	MODE	APER	CENWAV	DETECTOR	LAMP	DATE	TIME	PROPID	EXPTIME	CR
O44K05010	G430L	52X2	4300	CCDgain1	TU	04/11/97	19:28:02	7636	120.0	3
O44K05020	G430L	52X2	4300	CCDgain4	TU	04/11/97	19:34:08	7636	102.0	3
O44K06010	G430L	52X2	4300	CCDgain1	TU	02/12/97	17:43:08	7636	120.0	3
O44K06020	G430L	52X2	4300	CCDgain4	TU	02/12/97	17:49:14	7636	102.0	3
O44K08010	G430L	52X2	4300	CCDgain1	TU	26/01/98	03:52:17	7636	120.0	3
O44K08020	G430L	52X2	4300	CCDgain4	TU	26/01/98	03:58:23	7636	102.0	3
O44K09010	G430L	52X2	4300	CCDgain1	TU	23/02/98	03:12:30	7636	120.0	3
O4OZ01010	G430L	52X2	4300	CCDgain1	TU	23/02/98	04:29:25	7928	150.0	3
O44K09020	G430L	52X2	4300	CCDgain4	TU	23/02/98	03:18:36	7636	102.0	3
O4OZ01020	G430L	52X2	4300	CCDgain4	TU	23/02/98	04:36:01	7928	132.0	3
O4OZ02LLQ	G430L	52X2	4300	CCDgain1	TU	25/03/98	04:18:04	7928	50.0	1
O4OZ02LMQ	G430L	52X2	4300	CCDgain1	TU	25/03/98	04:20:16	7928	50.0	1
O4OZ02LOQ	G430L	52X2	4300	CCDgain1	TU	25/03/98	04:22:28	7928	50.0	1
O4OZ02LQQ	G430L	52X2	4300	CCDgain4	TU	25/03/98	04:24:40	7928	44.0	1
O4OZ02LSQ	G430L	52X2	4300	CCDgain4	TU	25/03/98	04:26:46	7928	44.0	1
O4OZ02LTQ	G430L	52X2	4300	CCDgain4	TU	25/03/98	04:28:52	7928	44.0	1
O4OZ03FSQ	G430L	52X2	4300	CCDgain1	TU	25/04/98	06:06:51	7928	50.0	1
O4OZ03FTQ	G430L	52X2	4300	CCDgain1	TU	25/04/98	06:09:03	7928	50.0	1
O4OZ03FUQ	G430L	52X2	4300	CCDgain1	TU	25/04/98	06:11:15	7928	50.0	1
O4OZ03FVQ	G430L	52X2	4300	CCDgain4	TU	25/04/98	06:13:27	7928	44.0	1
O4OZ03FWQ	G430L	52X2	4300	CCDgain4	TU	25/04/98	06:15:33	7928	44.0	1
O4OZ03FXQ	G430L	52X2	4300	CCDgain4	TU	25/04/98	06:17:39	7928	44.0	1
O4OZ05010	G430L	52X2	4300	CCDgain1	TU	23/06/98	00:01:56	7928	120.0	3
O4OZ05020	G430L	52X2	4300	CCDgain4	TU	23/06/98	00:08:02	7928	102.0	3
O4OZ06010	G430L	52X2	4300	CCDgain1	TU	23/07/98	05:36:07	7928	120.0	3
O4OZ06020	G430L	52X2	4300	CCDgain4	TU	23/07/98	05:42:13	7928	102.0	3
O4OZ07010	G430L	52X2	4300	CCDgain1	TU	22/08/98	00:33:56	7928	120.0	3
O4OZ07020	G430L	52X2	4300	CCDgain4	TU	22/08/98	00:40:02	7928	102.0	3
O4OZ08010	G430L	52X2	4300	CCDgain1	TU	21/09/98	05:16:07	7928	120.0	3
O53806030	G430L	52X2	4300	CCDgain1	TU	22/09/98	11:14:26	8080	30.0	3
O4OZ08020	G430L	52X2	4300	CCDgain4	TU	21/09/98	05:22:13	7928	102.0	3
O53806020	G430L	52X2	4300	CCDgain4	TU	22/09/98	11:09:50	8080	30.0	3

STIS Instrument Science Report 99-06

ROOTNAME	MODE	APER	CENWAV	DETECTOR	LAMP	DATE	TIME	PROPID	EXPTIME	CR
O4OZ09010	G430L	52X2	4300	CCDgain1	TU	21/10/98	02:21:37	7928	120.0	3
O4OZ09020	G430L	52X2	4300	CCDgain4	TU	21/10/98	02:27:43	7928	102.0	3
O53816020	G430L	52X2	4300	CCDgain4	TU	27/12/98	18:41:18	8080	30.0	3
O53816030	G430L	52X2	4300	CCDgain1	TU	27/12/98	18:45:54	8080	30.0	3
O53804010	G430L	52X2	4300	CCDgain4	D2	21/09/98	10:37:58	8080	60.0	3
O4LH03010	G230MB	50CCD	2557	CCDgain4	D2	05/03/98	07:04:08	7602	120.0	3
O4LH03020	G230MB	50CCD	2697	CCDgain4	D2	05/03/98	07:32:03	7602	93.0	3
O4LH03030	G230MB	50CCD	2794	CCDgain4	D2	05/03/98	07:59:31	7602	81.0	3
O4LH03040	G230MB	50CCD	2836	CCDgain4	D2	05/03/98	08:29:46	7602	75.0	3
O4LH04010	G230MB	50CCD	2976	CCDgain4	D2	05/03/98	04:43:37	7602	105.0	5
O4LH04020	G230MB	50CCD	3115	CCDgain4	D2	05/03/98	05:27:13	7602	70.0	5
O47Q06010	G430M	50CCD	5216	CCDgain4	TU	11/11/97	06:18:24	7666	9.0	2
O47Q06020	G430M	50CCD	5216	CCDgain4	TU	11/11/97	06:22:49	7666	27.0	2
O47Q06030	G430M	50CCD	5216	CCDgain4	TU	11/11/97	06:30:31	7666	36.0	2
O47Q06GQQ	G430M	50CCD	5216	CCDgain4	TU	11/11/97	06:16:53	7666	9.0	1
O47Q06GUQ	G430M	50CCD	5216	CCDgain4	TU	11/11/97	06:21:18	7666	9.0	1
O47Q06GXQ	G430M	50CCD	5216	CCDgain4	TU	11/11/97	06:26:01	7666	9.0	1
O47Q06H0Q	G430M	50CCD	5216	CCDgain4	TU	11/11/97	06:33:51	7666	9.0	1
O47Q06H1Q	G430M	50CCD	5216	CCDgain4	TU	11/11/97	06:35:22	7666	22.5	1
O47Q07010	G430M	50CCD	5216	CCDgain4	TU	11/11/97	06:48:10	7666	54.0	2
O47Q07H5Q	G430M	50CCD	5216	CCDgain4	TU	11/11/97	06:46:39	7666	9.0	1
O47Q07H9Q	G430M	50CCD	5216	CCDgain4	TU	11/11/97	06:51:48	7666	9.0	1
O47Q07HCQ	G430M	50CCD	5216	CCDgain4	TU	11/11/97	06:57:07	7666	9.0	1

Notes: 1. TU - Tungsten lamp. D2 - Deuterium lamp 2. CR - Number of readouts for cosmic ray rejection.

The production of flat fields that are locally normalized to unity follows the ACS cookbook of Bohlin, et al. (1999), with some modification. Standard bias and dark removal are adequate for these high S/N data. In particular, the steps required to make a pixel-to-pixel P-flat with the FLATS procedure are:

- a. Co-add similar illumination patterns with a cosmic ray rejection algorithm.
- b. Mask the edges of the data image and regions that have no valid data like the fiducial bar positions.

- c. Mask the dust motes, other blemishes that are smaller scale than  $\sim 50$ px, and the saturated pixels with  $\text{DN} > 32000$ . For STIS, the 32000 saturation limit at gain = 1 electron/DN is caused by non-linearity of the A/D amplifier and not by the CCD itself. At gain=4, saturation occurs at the CCD full well of 120,000 electrons, i.e. 30000 DN.
- d. Median filter each column of the data with a width of 13 pixels to remove the sharp features. A two-dimensional filter is not appropriate for those spectral images with the 52x2 slit that show deuterium emission lines.
- e. Fit the unmasked points in each filtered column of the flat field image with a spline function with 13 nodes.
- f. To avoid small discontinuities in the row direction (Bohlin, et al. 1999), iterate the fitting procedure of (d) by fitting the column fits with 13 node splines but in the row direction to make a final smooth fit image. This step must be skipped for the 52x2 deuterium spectra, where emission lines cause discontinuities in the spectral row direction, and for the G430L 52x2 tungsten spectra, which have a steep increase in signal with wavelength. When this step (f) is skipped, the initial column fit from step (e) must be used as the smooth approximation to the low frequency structure in the flat field observations. The errors introduced by skipping this second fitting are generally less than 0.1-0.2% and exceed one percent only rarely and only near the top and bottom edges of image, where the initial column fits are less well constrained.
- g. Divide the original, unmasked image by the smooth fit.
- h. Set to unity the masked points with no valid data or the lines where less than 55% of the data are valid for the spline fitting.
- i. Retain the statistical rms uncertainty image, as well as a data quality extension. Individual flats can be coadded using the statistical array for the proper weights and the data quality flags to ignore saturated and otherwise invalid regions.

In order to increase the statistical weight of the results and to investigate the characteristics of the CCD flats, the data from Table 1 are processed through the above steps a-i and then coadded with the COADD procedure and the appropriate statistical weights to produce the seven super flats in Table 2.

**Table 2.** COMBINED DATA SETS USED FOR CCD FLAT FIELDS

NAME	MODE	APERTURE	LAMP	IMAGES	OBS.	NOTES
PG430L-TUNG	G430L	52X2	TUNGSTEN	122	58	1,2a
PG230MB	G230MB	50CCD	DEUTERIUM	22	6	1,2b
PG430M-5216	G430M	50CCD	TUNGSTEN	16	12	1,2b
PG230LB-D2	G230LB	50CCD	DEUTERIUM	5	1	2a

NAME	MODE	APERTURE	LAMP	IMAGES	OBS.	NOTES
PG430L-D2	G430L	52X2	DEUTERIUM	3	1	2a
PGCCDL	...	...	...	160	76	3
PGCCDM	...	...	...	160	76	4

Notes: 1. Used to define the final pixel-to-pixel P-flat. 2. Used to define mote regions for a) low dispersion and b) medium dispersion. 3. Co-addition of the three sets with Note 1 and motes from sets with Note 2a. 4. Co-addition of the three sets with Note 1 and motes from sets with Note 2b.

The final two lines of Table 2 are the average recommended flat fields for all spectral observations in low dispersion (PGCCDL flat) and medium dispersion (PGCCDM flat). The rms Poisson statistics of PGCCDL and PGCCDM are 0.05-0.1%, i.e. signals of a few million electrons. See section 3.3 for details about the dust motes.

### 3. CHARACTERISTICS OF THE DATA

In order to characterize and quantify the properties of flat field data, the following software tools were developed:

- a. PRTIMG to display the flat images or ratios of images. See Figures 1-2 in Bohlin (1999) for the PGCCDL and PGCCDM examples. Visual examination of the flats or flat ratios with hard stretch like 0.98 to 1.02 show subtle problems with trial spline fits, saturation, masks, etc.
- b. STATS to tabulate the statistics in a pixel region (575:675,460:560) that is free of blemishes. Poisson counting statistics and rms scatter of the region are calculated for numerator, denominator, and ratio images. The Poisson scatter is removed in quadrature from the actual, measured sigmas to find the intrinsic rms statistical structure in the flats or in the ratio of the sub-images.
- c. FLTANAL to do the same as STATS, but plot the statistics as a function of X pixel all the way across the CCD for the strip of Y pixels (450:550).
- d. NCHANG to plot the results of STATS and display the statistical changes in the noise structure of the flats as a function of time.
- e. MODCF to illustrate the residual noise in extracted spectra by dividing the STIS spectra by stellar models that contribute no noise to the ratios.

#### 3.1. No Dependence on CCD Gain

STATS is used to create Table 3 from the monthly flat field monitor program. The one sigma Poisson counting statistics of the quantum events and the Actual one sigma rms scatter in the image are in Table 3 for the numerator, denominator, and ratio images. For the numerator and denominator images, the counting statistical scatter is removed from the Actual in quadrature to demonstrate the structure in the flat field itself (Sigma Flat) of

~ 0.8%, while the minimum and maximum values of the flat are indicated. In the ratio image, Residual Sigma is the one sigma scatter remaining after accounting for the contribution of the Poisson counting statistics, where a Residual =0 would signify a perfect flat field correction of the numerator by the denominator flat. The initial 5 digits of the first four column headings are the year and day number. In the final row of the Table, the rms residuals from a comparison of gain 1 vs. 4 on the same day in columns 3-4 are less than the residuals for the same gain on different days in columns 1-2. The fifth column compares the average of all G=1 with all G=4, G430L tungsten data from Table 1. This residual of <0.1% in column 5 demonstrates that the two commonly used gain settings produce practically identical flat fields. Gain 4 data is preferred for flat field images, because four times as many electrons per readout can be recorded. The final column compares two G=4 sets of data taken on the same day but at different exposure levels and demonstrates the invariance of the flat field over a range of ~3 in exposure. The signal levels range from ~8000 DN for the short exposures up to ~24000 DN for the longest exposure.

**Table 3. REPEATABILITY OF FLAT FIELD at G1 & G4**

	<b>97224G1</b>	<b>97224G4</b>	<b>97224G1</b>	<b>97251G1</b>	<b>ALL G1</b>	<b>SHORT</b>
<b>NUMERATOR</b>						
Poisson(%)	0.38	0.40	0.38	0.38	0.10	0.20
Actual sigma(%)	0.89	0.89	0.89	0.92	0.82	0.83
Sigma Flat(%)	0.81	0.80	0.81	0.84	0.81	0.81
Minimum	0.95	0.95	0.95	0.95	0.95	0.95
Maximum	1.03	1.03	1.03	1.04	1.03	1.03
	<b>97251G1</b>	<b>97251G4</b>	<b>97224G4</b>	<b>97251G4</b>	<b>ALL G4</b>	<b>LONG</b>
<b>DENOMINATOR</b>						
Poisson(%)	0.38	0.40	0.40	0.40	0.09	0.14
Actual sigma(%)	0.92	0.93	0.89	0.93	0.81	0.86
Sigma Flat(%)	0.84	0.83	0.80	0.83	0.80	0.85
Minimum	0.95	0.95	0.95	0.95	0.95	0.95
Maximum	1.04	1.05	1.03	1.05	1.03	1.03
<b>RATIO</b>						
Poisson(%)	0.54	0.57	0.55	0.55	0.13	0.24
Actual sigma(%)	0.60	0.62	0.57	0.57	0.15	0.25
Resid. sigma(%)	0.27	0.26	0.12	0.15	0.07	0.06

### ***3.2. The Flat Field Changes over Time but Is Independent of Wavelength.***

Despite the invariance of the CCD flat field, with wavelength (see below and section 4), gain, and signal level, the CCD is not a perfect detector. The flat field shows significant changes with time in orbit. Figure 1 from NCHANG.pro shows that the intrinsic rms scatter in the G430L tungsten flats increases from 0.8 to  $>0.9\%$  from the start of orbital operations to the end of 1998. More relevantly, Figure 2 demonstrates that the intrinsic residual rms structure after flat field correction increases with the time difference between numerator and denominator flats. For pairs of flats taken on the same day and plotted at day=0, the residual is only  $\sim 0.1\%$ , while the residual gradually increases from  $\sim 0.3\%$  for a time difference of a month to  $>0.6\%$  as the time difference exceeds 1.5 years. To avoid possible pathological choices for a single denominator flat, the observations are compared pair-wise over the observation period of Figure 1. For example, the last point at day 620 is the residual between the first monthly flat on 97104=97Apr14 and the last observation of 1998 on 98361=98Dec27, while the data points at day 27 and 28 and are comparisons between dates of 97224 and 97251 and between 98026 and 98054, respectively.

Figure 2 suggests that a S/N of 1000 per pixel with the STIS CCD can be achieved with a contemporaneous flat that has at least a million electrons. The average flats PGC-CDL and PGCCDM from Table 2 leave systematic residuals of 0.2-0.4% per pixel for data taken before 1999.0. After 1999.0, these early flats will introduce systematic noise exceeding 0.4% rms per pixel. Since these new flats will be out of date and may even be worse than no flat at some point in time, a new spectral flat monitoring program begins in the second half of 1999 and will obtain monthly CCD flats at a typical signal level of about a half million electrons. Possibly, the existing monitoring for imaging with the MIRVIS could produce monthly flats with sufficient S/N for the period before 1999. Only data from the spectral-flat proposals have been examined for this ISR.

One other alternative to achieving a S/N of 1000 per pixel with the STIS CCD might be to dither the stellar spectrum along the slit. For example, nine dither positions should reduce a systematic flat fielding error of 0.3% to 0.1%. The total rms scatter should be the combination of this 0.1% residual with the Poisson statistics of the sum of the data from the nine positions.

The high S/N flats in the first five lines of Table 2 are intercompared with FLTANAL to measure the residual rms scatter across the center of the CCD. None of the residuals exceed the amount predicted from Figure 2 for the difference in time, i.e. there is no extra residual caused by the different spectral distribution of the light hitting each pixel. For example, the ratio of PG430M-5216 taken on 97Nov11 with a tungsten source and the 50CCD aperture divided by PG230MB or PG430L-D2 has rms residuals of  $\sim 0.35$  or  $0.5\%$  for time differences of 114 or 314 days, respectively. Thus, the change in illuminating spectrum from tungsten to the deuterium lamp for both PG230MB and PG430L-D2 and to the purer spectrum of the 52x2 slit for PG430L-D2 does not increase the residuals predicted by Figure 2 for the time difference of 114 or 314 days.

Figures 3-4 illustrate the above conclusion for a part of row 509, which often intersects the first order CCD spectra. Figure 3 shows the same triple pattern of low flat field response of 0.95-0.98 for a variety of observation modes and illuminating flat field lamp, all obtained within the month from 98Feb23 to 98Mar25. Figure 4 illustrates the development of this triple pattern from before launch in 1996 to 98Sep21. The use of a pre-launch flat causes errors of  $>5\%$  by 98Sep, e.g. at pixel (144,509). An even more variable pixel that affects spectra is (77,512), which drops in sensitivity by 10% from 1996 to 98Mar. In this text, the counting of the pixels in a STIS image is based on the index of one for the first pixel, rather than on the IDL convention of zero used for the plots.

### ***3.3. Motes and Blemishes***

The CCD has 84 regions of reduced sensitivity due to dust particles on the detector window or to blemishes on the CCD itself (Bohlin 1999). The bulk of these are dust motes, which show reduced sensitivity by a few percent, typically, although the mote at (80,648) has a central response of  $\sim 0.7$  in low dispersion. In medium dispersion, the different optical magnification makes the dust motes shallower; and their centroids are shifted left by two pixels. PGCCDL motes have diameters of 24 pixels, while the PGCCDM motes are 32 pixels in diameter. Except in the regions of the 84 motes, the flats PGCCDL and PGCCDM are identical. Since the flat fields do not correct narrow stellar spectra perfectly at the positions of motes and leave residuals up to 3%, the mote regions are flagged in the bad pixel table and in extracted spectra so that these artifacts are not mistaken for real spectral features.

## **4. STELLAR SPECTRA**

In order to evaluate the effectiveness of the flats, the sets of eight GD153, two or four G191B2B, and seven AGK+81D266 low dispersion stellar spectra from the Sensitivity Monitoring Program (Walborn and Bohlin 1998) are reduced with various flat field options and coadded to increase S/N. Spectra are extracted from flat fielded images as the sum of the signal in the standard extraction height of 7 pixels. The process of coadding rows of an image reduces the noise by more than expected from Poisson statistics. The 0.8-0.9% rms structure of the flats shown in Table 3 and Figure 1 is reduced by more than the expected factor of 2 for the coaddition of 4 rows. For example, FLTANAL results show that PGCCDL has an rms of 0.80%, while the rms of the flat binned over 4 rows is 0.30%, instead of the expected 0.40%. Therefore, there must be some correlated noise from row to row. The low rms structure of 0.80% in the CCD flat itself, the binning over 7 rows, and the correlated noise all conspire to reduce the intrinsic rms noise in stellar spectra that are extracted WITHOUT any flat field. Simulated stellar images with infinite S/N and proper weighting for each of the 7 lines are corrected with the high S/N PGCCDL flat. The simulated spectra show intrinsic rms noise of only 0.25-0.35%, depending on how the point source is sampled by the CCD pixels. Therefore, spectra extracted from images with NO

flat fielding will be dominated by Poisson noise, unless at least  $\sim 100,000$  electron events are available. Flat fields are potentially useful for stellar spectra only in these high S/N cases. Flats will start to reduce diffuse source noise significantly as signal levels rise above 16,000 electrons/px.

Because of the variability of the CCD flat field with time and the availability of only time average flats, a GO should always check the reality of weak spectral features by extracting the spectrum with OMIT for the flat field processing step. The mean weighted time of observation for the PGCCDL and PGCCDM flats is early in 1998; and the best flat field correction is for data taken in the same time frame. For example, Figure 5 is a MODCF plot of residual noise level for various flat fields in a wavelength region where there are  $\sim 1,300,000$  electrons/px in the stellar spectrum. Because the observation of the four G191B2B spectra are all in the 97Oct-98Feb time frame near the mean time of the flat, the new PGCCDL flat improves the rms from the 0.33% with no flat to 0.24%, i.e.  $S/N=417$ , which is probably still dominated by the systematic error introduced by applying an average flat to data obtained at a different mean time. In the center panel of Figure 5, the pre-flight flat that has been used to reduce all archival data makes the rms slightly worse than with no flat at all. As time from launch increases, the pre-flight flats produce progressively larger flat fielding errors in STIS CCD spectra.

Figure 6 is a case where the application of the PGCCDL flat is worse than no flat, because the spectra are taken shortly after launch with a mean date of 97Jun. In particular, the spike of 1.013 at  $3094\text{\AA}$  is caused by the rapid loss of sensitivity of the pixel (77,512), (index 1 based). This pixel should be added to the bad pixel list, unless a monthly flat field correction procedure is established. Unit sensitivity at launch, this pixel dropped to 0.9 by 98Mar. Thus, the 97Jun spectrum of GD153 has been overcorrected by the PGCCDL flat field with its mean date early in 1998.

Finally, Figure 7 illustrates a case where the pre-flight pipeline flat has a low S/N, which makes the corrected spectrum GD153.G430L-ORIG much worse than with no flat at all. The new PGCCDM flat leaves a residual rms of 0.44% in this line free region of BD+75D325, while the no-flat rms is better at 0.35%. Even though the early 1998 epoch PGCCDM flat is not the most appropriate correction for the BD+75D325 spectra obtained in May97, the high S/N PGCCDM is superior to the pre-flight flat. The Poisson noise in the BD+75D325 spectrum is 0.25%, while the inadequate statistics of the pre-flight flat for G430M-4451 are  $\sigma=1.01\%$  per pixel. The average rms statistical noise in the central  $200 \times 200$  pixels of the CCD flats at the primary grating settings are provided in Table 4 as guidance on whether any particular data set would benefit from reprocessing with one of the two new PGCCD flats. Since the structure that the flat field should remove is only  $\sim 0.8\%$ , those five flats with Poisson noise greater than 0.8% have always degraded the S/N in archival, pipeline processed spectra. Those eight flats with rms between 0.6 and 0.8% will often degrade the results depending on the time from launch and on the number of artifacts in these individual flat fields. Little improvement will result from reprocessing of

the four modes in Table 4, where ‘none’ indicates default processing with no flat field.

**Table 4.** Flat Fields for the CCD Primary Modes

Mode	Centwave (Å)	Central rms (%)
PGCCDL	...	0.066
PGCCDM	...	0.066
G230LB	2375	0.72
G430L	4300	0.26
G750L	7751	none
G230MB	1713	none
G230MB	1854	none
G230MB	1995	none
G230MB	2135	0.79
G230MB	2276	0.44
G230MB	2416	0.90
G230MB	2557	0.58
G230MB	2697	1.23
G230MB	2836	0.80
G230MB	2976	0.55
G230MB	3115	0.65
G430M	3165	0.38
G430M	3423	0.56
G430M	3680	0.76
G430M	3936	0.48
G430M	4194	1.21
G430M	4451	1.01
G430M	4706	0.82
G430M	4961	0.57
G430M	5216	0.62
G430M	5471	0.61
G750M	5734	0.31
G750M	6252	0.36
G750M	6768	0.39
G750M	7283	0.36

<b>Mode</b>	<b>Cenwave (Å)</b>	<b>Central rms (%)</b>
G750M	7795	0.37
G750M	8311	0.40
G750M	8825	0.35
G750M	9336	0.32
G750M	9851	0.35
G750M	10363	0.63

Starting with G750M-6252, fringing becomes an increasingly worse flat field problem toward longer wavelengths and dominates the flat field structure. Since the fringe pattern is broad and stable, separate flats for each G750M mode should continue to be used in pipeline processing. No updates of these 10 pre-flight flats are provided at this time. To provide the pixel-to-pixel correction without introducing extraneous noise, the high S/N PGCCDL flat should be applied for G750L along with a contemporaneous flat to remove the long wavelength fringing (Goudfrooij, et al. 1998). That de-fringing procedure remains the same, except for the replacement of the pixel-to-pixel correction with the 50 CCD flat by the higher S/N PGCCDL flat. No flat field data with any fringing have been included in the new PGCCD flats.

PGCCDL is the new flat field for the three low dispersion CCD spectral modes, while PGCCDM should be used for all G230MB and G430M modes.

## 5. ACKNOWLEDGEMENTS

Thanks to D. Lindler, H. Ferguson, R. Gilliland, and L. Dressel for corrections and constructive comments.

## 6. REFERENCES

- Bohlin, R. 1999, Instrument Science Report, STIS 99-04, (Baltimore: STScI).
- Bohlin, R., Hartig, G., Lindler, D., Meurer, G., & Cox, C. 1999, Instrument Science Report, ACS 99-01, (Baltimore: STScI).
- Goudfrooij, P., Bohlin, R., Walsh, J., & Baum, S. 1998, Instrument Science Report, STIS 98-19, (Baltimore: STScI).
- Walborn, N., & Bohlin, R. 1998, Instrument Science Report, STIS 98-27, (Baltimore: STScI).

## 7. FIGURES

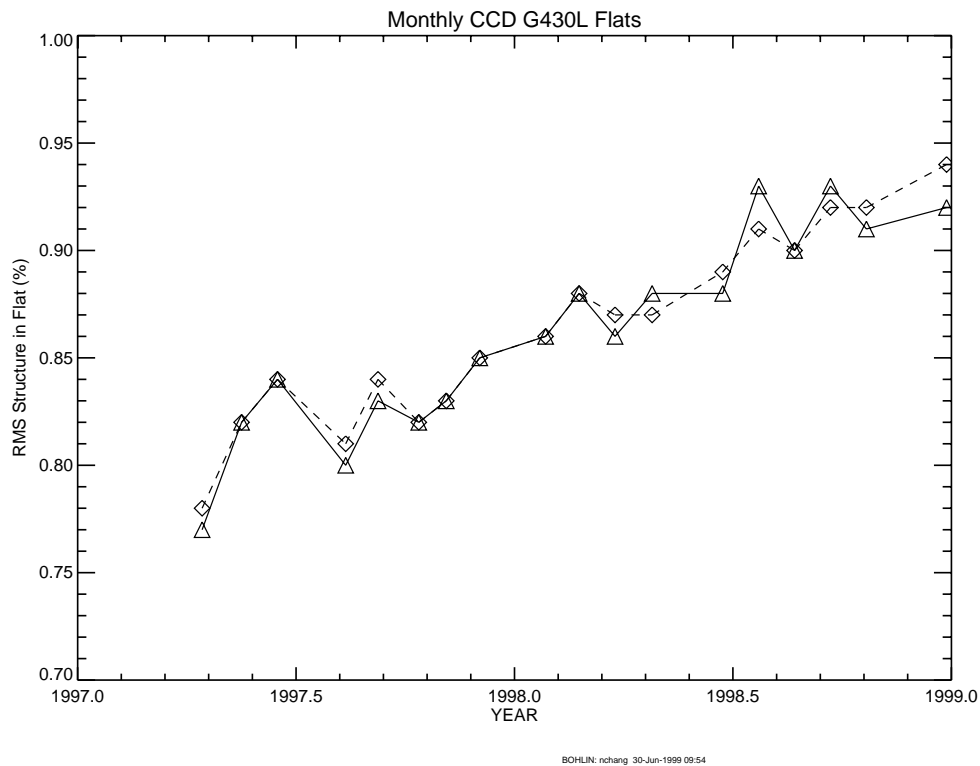
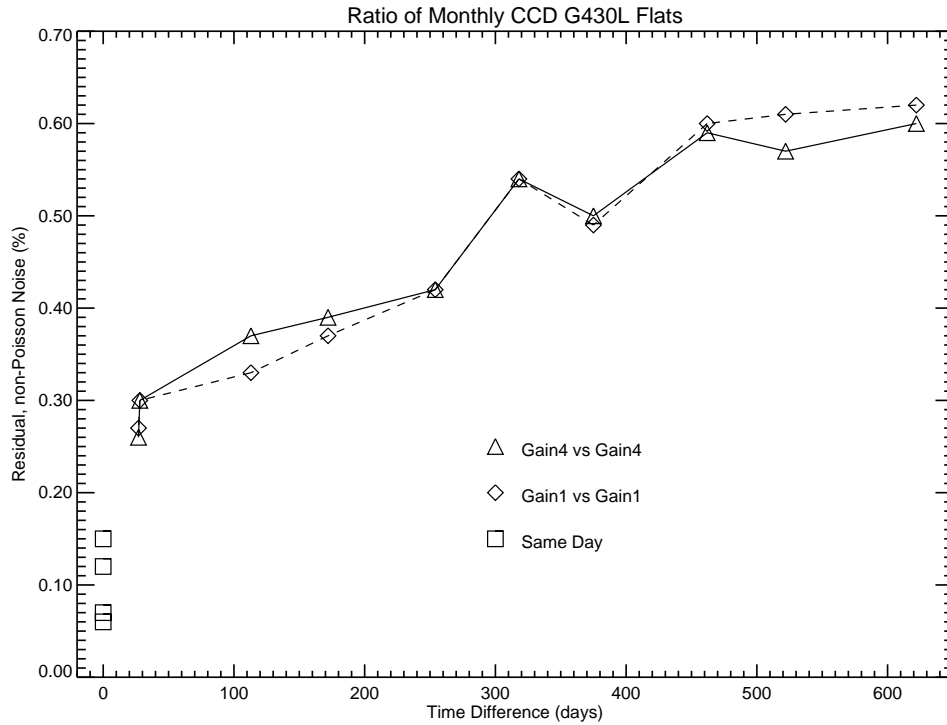


**Figure 1:** Intrinsic rms structure in the monthly G430L 52x2 tungsten flats. Triangles connected with the solid line are for gain=4, while the diamonds and dashed line are for gain=1. The two gain settings produce nearly identical results. The Poisson counting statistics have been removed in quadrature from the measured rms scatter of the region (575:675,460:560) to produce the plotted residuals.



BOHLIN: nchang 30-Jun-1999 09:52

**Figure 2:** Residual rms structure in a flat field after correction by another flat as a function of the time difference between numerator and denominator flats. The triangles and diamonds are as in Figure 1, while the squares are for data taken on the same day. At a time difference of  $\sim 0$ , the residual is only  $\sim 0.1\%$ , while the residual gradually increases from  $0.3\%$  after a month to  $>0.6\%$  for a time difference of more than 1.5 years.  
 /home/bohlin/ccdfit.fig3

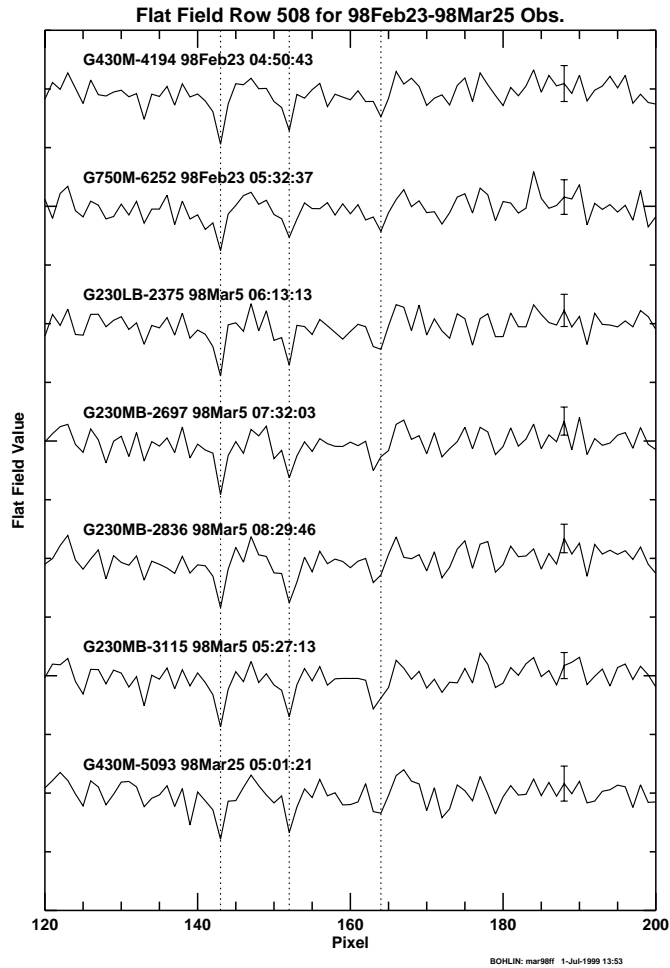


**Figure 3:** Flat field at pixels (120:200,508) near the region of the first order CCD spectra for a variety of modes and illuminations in the month 98Feb23-98Mar25. Each observation is normalized to unity, while the y-axis increments are 0.05. Vertical dotted lines at pixels 143, 152, and 164 mark locations of low flat field response. A typical 3-sigma uncertainty is shown by the error bar at x-pixel 188. The different observational modes have the same flat field to within the uncertainties. Pixels are counted on the IDL convention starting with zero for this figure and caption. Add one for the IRAF convention.

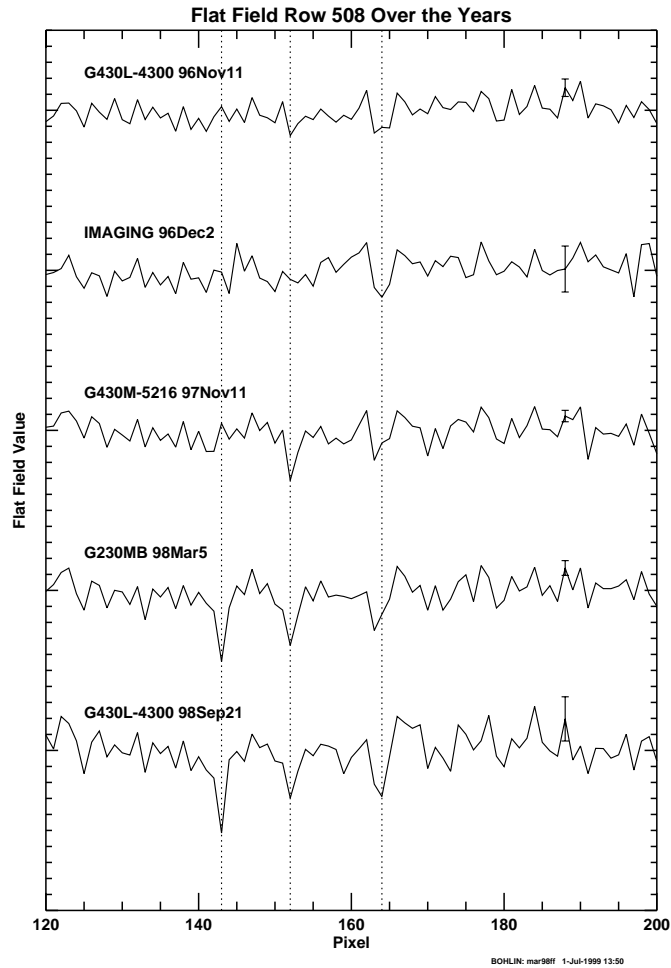


**Figure 4:** As in Figure 3, except for a range of times covering almost 2 years. The flat field level at x-pixels 143 and 152 decreases with time, while the feature at x=164 is more constant. For data taken in the fall 1998 time frame and corrected with a pre-flight lab flat, the pixel (143,508) values are ~5% low.

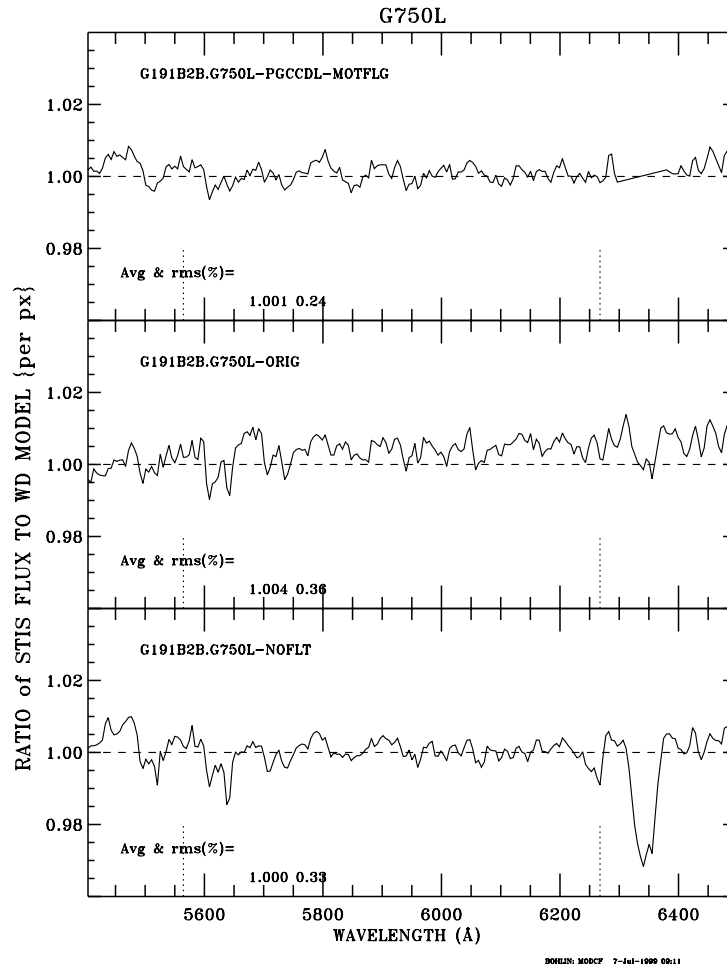


**Figure 5:** The sum of four G430L spectra of G191B2B obtained in the 97Oct-98Feb time frame. Plotted as a function of wavelength is the ratio of the STIS data to the noiseless model spectrum for that standard star. There are no features in the standard spectrum, while the dip in the 6350Å region of the lower panels is a dust mote in the data. The lowest panel (G191B2B.G750L-NOFLT) has no flat field; G191B2B.G750L-ORIG is with the original current pipeline flat from pre-launch data; and G191B2B.G750L-PGCCDL-MOTFLG is the new flight flat with the mote region flagged, so that the region of the mote can be automatically ignored. The two numbers at the lower left of each panel are the mean level and rms scatter in percent of the data points in the 5565-6268Å region delimited by the short vertical dotted lines. The new flat produces the best signal-to-noise ratio with a  $\sigma=0.24\%$  or  $S/N=417$ . The quantum statistical limit is 0.09% from the Poisson noise in the data.

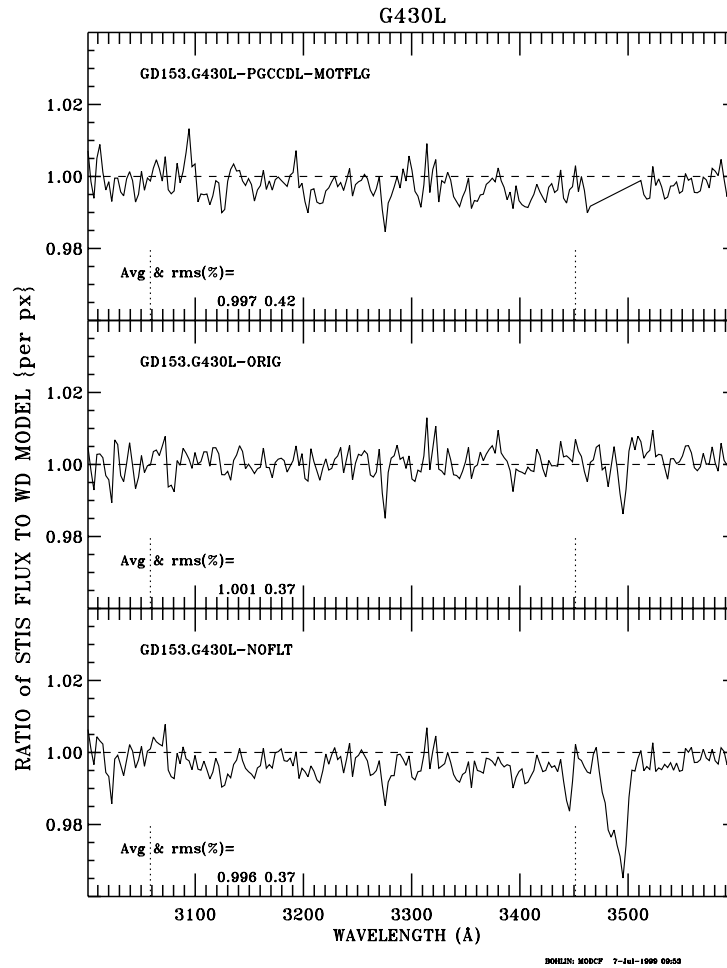


**Figure 6:** As in Figure 5 for the sum of eight spectra of GD153 with mean time of observation in 97Jun. The dip just shortward of 3500Å is the dust mote, while the wavelength range for the rms statistics is 3059-3451Å. Because of the difference in the mean time of the flat and the mean observation time of the data, the new PGCCDL flat makes the noise slightly worse; and the original pre-flight flat has a noise level that is the same as for no flat. The quantum statistical noise of 0.3% dominates the stellar spectrum.

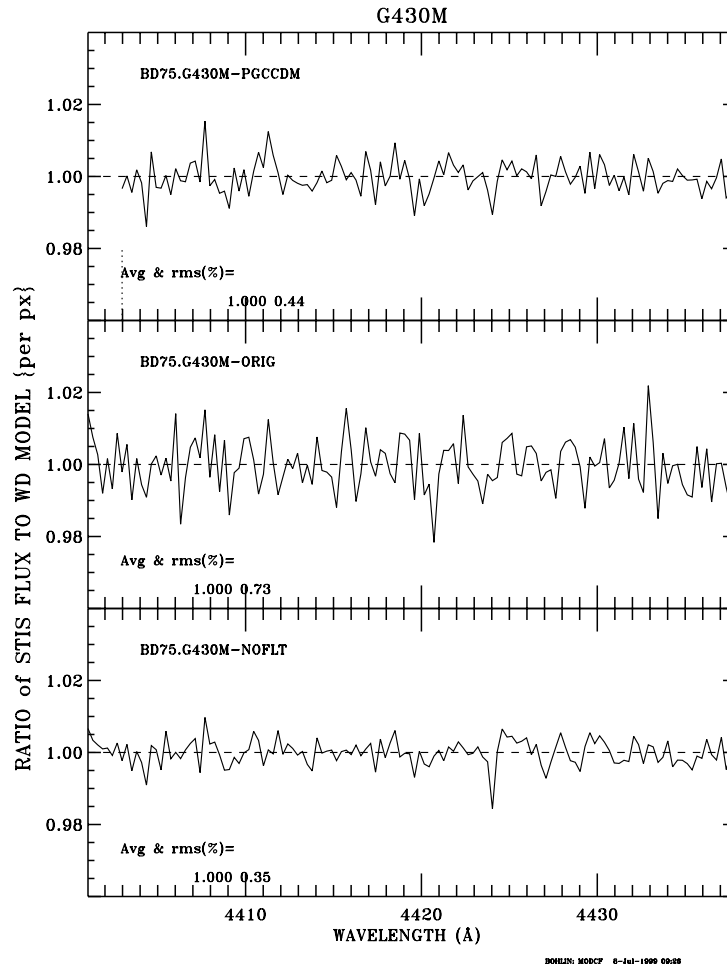


**Figure 7:** As in Figure 5 for the sum of four G430M spectra of BD+75D325 observed on 97May18. Instead of comparing to a theoretical model for the flux distribution of BD+75D325, the spectrum is divided by a heavily smoothed version of itself. The original pre-flight flat degrades the S/N because of its low statistical significance.